A Pixel Based Regeneration Index using Time Series Similarity and Spatial Context

Stefaan Lhermitte, Jan Verbesselt, Willem W. Verstraeten, and Pol Coppin

Abstract

Although the regeneration index based on control plots provides a valuable tool to quantify fire impact and subsequent vegetation regrowth, the practical implementation at large scale levels remains limited due to the need for detailed reference maps. The objective of this research therefore was the development of an image-based selection approach for control pixels based on time series similarity (TSS). The TSS approach allows the computation of a per-pixel regeneration index on regional to global scale without the need for reference maps. Evaluation of the control plot selection approaches based on un-burnt focal pixels confirmed the validity of the TSS approach and showed optimal results for the TSS_{RMSD} approach with $x = 4$ and $N_T = 8$ due to beneficial averaging effects and minimal window size effects. As such, the effects of spatial heterogeneity and noise are minimized and a preliminary quality indicator can be derived.

Introduction

Large scale vegetation fires are a determining factor in the dynamics of almost all terrestrial ecosystems (van Wilgen and Scholes, 2000). The environmental effects of these fires are enormous, as the biomass burning translates in a partial or complete destruction of vegetation cover, instigating abrupt changes in the ecological processes (Ehrlich *et al.*, 1997) and carbon fluxes (Lambin *et al.*, 2003). Accurate methods for assessing the fire event and describing the spatio-temporal post-fire vegetative development are consequently essential to understand the impact of vegetation fires and to estimate the changes of terrestrial ecosystems after fire.

Several remote sensing studies have discussed the potential of vegetation indices (VI), such as the normalized difference vegetation index (NDVI), to quantify the fire impact and vegetation recovery. Various approaches were introduced to interpret these indices, ranging from visual assessment (Marchetti *et al.*, 1995), to textural analysis (Chuvieco, 1999; Ricotta, 1998), multi-temporal classification comparison (Espírito-Santo *et al.*, 2005; Hayes and Sader, 2001; Kimes *et al.*, 1999) and time series analysis. Time series analysis showed particularly useful because the change curve of vegetation growth reveals important information about ecosystem functioning (Lawrence and Ripple, 1999). Accordingly, three time series analysis techniques have been proposed in literature to describe the vegetation regrowth. The first one is based on the temporal evolution of post-fire VIs without any reference to the situation prior to the fire event (Fiorella and Ripple, 1993). The second approach relates the post-fire growth to pre-fire situations using the difference or ratio in VIs before and after the fire occurrence (Henry and Hope, 1998; Hicke *et al.*, 2003; Kushla, 1998; Viedma *et al.*, 1997; White *et al.*, 1996). Both these approaches however are very sensitive to normalization of the image data for noise factors, including radiometric calibration uncertainty, errors in the atmospheric correction, bidirectional reflectance distribution function (BRDF) effects, topographic impact, and shifts in the phenological state of the vegetation between data acquisition times (Riaño *et al.*, 2002). Song (2002) highlighted the reduction of these kinds of image noise as the primary challenge when using multi-temporal imagery to monitor forest regrowth. Moreover, Viedma *et al.* (1997) and Song (2003) stressed the need for phenological and seasonal corrections to interpret long-term regrowth of the vegetation communities. Hence, a third approach based on continuous monitoring with control plots was proposed to solve these problems (Díaz-Delgado *et al.*, 2003; Díaz-Delgado and Pons, 2001; Díaz-Delgado *et al.*, 1998; Riaño *et al.*, 2002). It is based on a regeneration index (RI) that employs information of control plots located close to but unaffected by the fire, to correct for external influences and phenological variation:

$$RI^t = \frac{VI^t_{fire}}{VI^t_{control}} \tag{1}$$

where RI^t is the mean regeneration index at moment t, VI^t_{fire} is the mean vegetation index of the fire plot pixels at moment t, and $VI^t_{control}$ is the mean vegetation index of the control plot pixels at moment t. RI^t values of one can be expected when the fire and control plot show identical vegetation growth, whereas RI^t values above or below one indicate lower or higher VI^t values for the fire plot in

Stefaan Lhermitte is with Centro de Estudios Avanzados en Zonas Aridas (CEAZA), Universidad de la Serena, Casilla 599, La Serena, Chile, and formerly with M3-BIORES, Biosystems Department, Katholieke Universiteit Leuven, Heverlee, Belgium (lhermitte.stefaan@ceaza.cl).

Jan Verbesselt is with CSIRO Sustainable Ecosystems, Private Bag 10, Clayton South, VIC 3169, Australia.

Willem W. Verstraeten, and Pol Coppin are with M3-BIORES, Biosystems Department, Katholieke Universiteit Leuven, Willem de Croylaan 34, BE-3001 Heverlee, Belgium.

Photogrammetric Engineering & Remote Sensing
Vol. 76, No. 6, June 2010, pp. 673–682.

0099-1112/10/7606–0673/$3.00/0

comparison with the control plot. The RI approach is founded on the assumption that the vegetation growth of the control plots can serve as an indicator for vegetation growth in case the fire had not occurred. As such, external influences can be masked out and the variation in RI can be interpreted solely due to regeneration processes. The correct selection of control plots is critical in this approach to avoid relating RI changes to other site differences. For example, Riaño *et al.* (2002) combined local information and detailed vegetation reference data (describing vegetation communities, patch sizes, climatic conditions, distance to the sea, and topographic position) to select control plots that did not burn, with similar environmental conditions and vegetation state, ideally located adjacent or close to the burnt sites.

The RI has however two difficulties for large scale fires. First, large scale application of the RI on regional, continental, or global scale remains constrained due to the lack of detailed local reference data and the limitations of coarse scale reference maps. The use of reference maps at these coarse scale levels, for example, often introduces ecological and site differences, which impede correct application and interpretation of the RI for regrowth assessment. This is evident in the study of Goetz *et al.* (2006), who employed a control plot selection approach based on a regional ecoregion map and low coefficients of variation across coarse spatial resolution AVHRR image time series. The results revealed severe site differences between burnt and control plots, as the $VI^t_{control}$ fails to provide the temporal profile of the fire plot before the fire event. Consequently, the interpretation of the RI for regrowth assessment is complex, since the RI contains variation not caused by the regeneration process. Fraser *et al.* (2000), on the other hand, employed the RI on coarse SPOT-VEGETATION (VGT) data using control plots based on Landsat TM scenes. Although this approach is promising, it requires fine resolution Landsat imagery, which is obtained infrequently over small areas (Cihlar, 2000). Consequently, difficulties arise to cost-effectively obtain control plots over large areas in rapidly changing environments. Second, the RI fails to describe the heterogeneity of regrowth in each fire plot due to the use of mean values per fire plot. Nevertheless, the heterogeneity within a burnt area can be large in terms of vegetation growth prior to the fire and fire impact (Alleaume *et al.*, 2005), resulting in a heterogeneous regrowth that cannot be detected by current RI application.

Consequently, the objective of this paper is to develop an approach for the image based selection of control pixels for each fire pixel on regional to global scale. This approach allows the calculation of a pixel based regeneration index (pRI):

$$pRI^t = \frac{VI^t_{focal}}{VI^t_{control}} \quad (2)$$

where pRI^t is the pixel based regeneration index at moment t, VI^t_{focal} is the vegetation index of the focal or central fire pixel at moment t, and $VI^t_{control}$ is the mean vegetation index of the selected control pixels at moment t. The pRI will allow quantifying the heterogeneity within a fire plot, since each fire pixel is considered independently as focal or central study pixel and control pixels are selected specifically from a selection window around that focal pixel. In this framework, an alternative time series similarity approach (TSS) for control pixel selection is proposed that combines time series similarity measures with spatial context constraints. The TSS approach is independent of static reference data and allows the extraction of control pixels over large areas for each focal pixel.

In this paper, the TSS approach is evaluated using un-burnt focal pixels, since the use of un-burnt focal pixels allows the quantitative assessment of temporal similarity between VI^t_{focal} and $VI^t_{control}$ in case the fire had not occurred. As such, a sensitivity analysis of the TSS approaches to selection parameters can be performed, and the TSS approaches can be compared to the classic reference map approach. Moreover, quality indicators can be derived to assess the accuracy of the pRI in future research.

Study Area and Data

Study Area

All approaches for control pixel selection were applied on the area of South Africa, Swaziland and Lesotho, which approximately encompasses the geographic region between latitudes 21° S and 35° S and longitudes 33° W and 16° E. The study area was selected based on the broad range of ecosystems and fire regimes that influence the fire impact and vegetation regrowth. The ecosystems vary from grasslands, to forest, cultivated land and woodland savanna (Tainton, 1999). Fire activity typically starts with the onset of the dry season in May and extends untill October (Silva *et al.*, 2003). Elevation ranges from sea level to more than 3,300 m, while the rainfall varies from almost zero to more than 3,000 mm in mountainous areas. Rainfall regimes are defined as winter rainfall in the west to strong summer rainfall regimes in the northeastern and northern parts of the study area.

Satellite Data

Analysis for this work was performed on ten-daily normalized difference vegetation index (NDVI) image composites (S10) from the SPOT-VEGETATION (VGT) sensor. Preprocessing of the data was performed by the Vlaamse Instelling voor Technologisch Onderzoek (VITO) in the framework of the Global Vegetation Monitoring (GLOVEG) preprocessing chain. It consisted of the Simplified Method for Atmospheric Correction (SMAC) (Rahman and Dedieu, 1994) and compositing at ten-day intervals based on the Maximum Value Compositing (MVC) criterion (Holben, 1986). The final data set consisted of 270 ten-daily, 1 km resolution NDVI S10 composites for the period 01 April 1998 to 30 September 2005 with additional surface reflectance values in the blue (B; 0.43 to 0.47 μm), red (R; 0.61 to 0.68 μm), near-infrared (NIR; 0.78 to 0.89 μm) and shortwave-infrared (SWIR; 1.58 to 1.75 μm) spectral bands. From this data set only the NDVI (in the TSS approach) and B (for post-processing) observations were used.

The geometric and radiometric corrected VGT S10 time series were postprocessed to remove cloud observations that possibly corrupt satellite observations. The cloud mask consisted of masking pixels using an adapted threshold approach based on Kempeneers *et al.* (2000) and Verbesselt *et al.* (2006). A pixel was classified cloud-free, if the blue reflectance was less than 0.075, and no error flags were present in the status map. All erroneous data were finally replaced by no-data values and as such omitted in any further processing.

Vegetation Map

A regional reference data set was employed in the classical reference map approach for control pixel selection that is contrasted with the TSS approaches. The intersection of Low and Rebelo's (LR) Vegetation Map of South Africa, Lesotho and Swaziland (Low and Rebelo, 1996) and the National Land-cover (LC) map of South Africa (Thompson, 1999) were used for this purpose. This LR/LC intersection

combines information of ecosystem potential, vegetation structure, plant species, and ecological processes, with information on actual vegetation and dominant land-cover/land-use type. It was created from field surveys and high-resolution imagery at the 1 km sub-pixel level, but was resampled to represent the dominant LR/LC unit per 1 km pixel.

Burnt and Un-burnt Areas

Burnt and un-burnt pixels of the year 2000 were identified from the overlap of the burnt areas derived from the Global Burnt Area 2000 (GBA2000) and the Globscar initiative. The former is a fire scar inventory performed by the Joint Research Centre (JRC) based on different regional algorithms for temporal and spatial subsets of VGT S1. The Southern Africa data set, for example, was derived from monthly composites to obtain substantially cloud-free images (Silva *et al.*, 2003). Burnt areas were identified from these monthly composites using a classification tree that relied on the VGT NIR channel. The resulting product contains the area burnt on a monthly basis without providing the date of fire detection. The Globscar product, on the other hand, was developed by the European Space Agency (ESA) using Along Track Scanning Radiometer (ATSR-2) daytime data of the year 2000. The product combines the result of two algorithms for burnt area detection: the K1 algorithm based on the geometrical characteristics of the burnt pixels in the NIR and thermal infrared (TIR) space, and the E1 algorithm derived from four different spectral channels (Simon *et al.*, 2004). The final product is available at monthly intervals, but provides for each burnt pixel also the date of fire detection.

Although fire inventories theoretically should produce identical burnt pixels, the area detected by GBA2000 in South Africa is three times larger than the burnt area detected by Globscar (Simon *et al.*, 2004). In this paper, the combination of both maps served as a solution to this problem and the issue of false detection. A pixel was classified burnt or un-burnt if it satisfied, respectively, the burnt and un-burnt classification of both the GBA2000 and Globscar algorithms simultaneously. This is not an optimal solution for burnt and un-burnt area assessment, but an improved burnt map can be used as better fire inventories become available. However, the accurate amount of burnt pixels is not important in the framework of this study, since we are interested in the development of a methodology for reference area selection and the combination of both maps allows the validation of the methodology on pixels with a higher burning or non-burning certainty.

Control Plot Selection Approaches

For valid pRI estimates, control pixels must correspond to the fire pixel in case the fire had not occurred. First, this implies identical pre-fire vegetation characteristics for both focal and control pixels as defined by the selection criterion (see the following sub-sections). Second, it means similar post-fire environmental conditions, since the pRI assumes identical vegetation growth in case the fire had not occurred. The TSS approach is presented in this paper as an alternative for the classical reference map approach to select control pixels that fulfill these requirements.

Reference Map Approach

In the classic reference map (REF) approach that was previously used for the RI, un-burnt control pixels are selected based on reference maps. Goetz *et al.* (2006), for example, used a coarse ecoregion map based on climate, physiography, and existing ecological information, whereas other authors (Díaz-Delgado *et al.*, 2003; Díaz-Delgado and Pons, 2001; Riaño *et al.*, 2002) combined vegetation maps with spatial neighborhood constraints. Spatial neighborhood is incorporated to constrain the candidate control pixels based on post-fire environmental conditions. Spatial neighborhood does not guarantee any post-fire similarity, but it maximizes the probability of having similar post-fire environmental conditions. This can be explained by the spatial dependence of many of these environmental conditions (e.g., climate, weather, soil, topography), which is high for short distances and dissipates into randomness for large distances. This similarity at short distances is used in the REF approach, since all un-burnt pixels around the focal pixel with similar reference map characteristics (e.g., LR/LC reference map characteristics) are selected to calculate the $VI^t_{control}$. Based on the $VI^t_{control}$, the pRI^t_{REF} can be calculated for every focal pixel.

Time Series Similarity Approach

The proposed TSS approach is a multi-temporal selection approach that combines time series similarity and spatial context to select control pixels. Various authors have already demonstrated the power of similarity of yearly VI^t time series to discriminate between land-cover/land-use types and ecosystem state (Defries *et al.*, 1995; Justice *et al.*, 1985; Loveland *et al.*, 2000; Reed *et al.*, 1994; Viovy, 2000). This discrimination power of one year VI^t time series is now employed to select control pixels with similar pre-fire vegetation characteristics.

The TSS approach is a selection approach that uses the central study or focal pixel as selection seed. Based on this seed pixel p, a first run is started that compares p with its spatial adjacent pixels that did not burn. This comparison is based on a dissimilarity criterion S that quantifies the time series similarity of one year VI^t before fire occurrence. This results in N_x candidate control pixels. Subsequently, N_x is compared with a user-defined threshold value N_T. If $N_x < N_T$, an iterative run is started to increase the number of candidate control pixels N_x. This is done by increasing the spatial neighborhood window around p with one pixel on each side (e.g., from a 3 by 3 window to a 5 by 5 window). In this larger window, p is compared with the N_x candidate control pixels that did not burn based on S. If again $N_x < N_T$, the iterative run is repeated by increasing the spatial neighborhood window around p. This process of iterative runs continues until $N_x \geq N_T$. Subsequently, a user-defined number of pixels x is selected from these N_x candidate control pixels, that show the highest temporal similarity with p in the one year VI^t before the fire. These x selected control pixels finally allow the calculation $VI^t_{control}$ and pRI^t_{TSS}.

The TSS is a generalized approach for control plot selection that can be applied on any satellite image time series. The outcome will depend however strongly on the selection of the dissimilarity criterion S. Therefore, the performance of two similarity measures for the TSS approach was compared: TSS_{CC} based on cross-correlation (CC) and TSS_{RMSD} based on the root mean square distance (RMSD). The cross-correlation (CC) for two time series $f^p(t)$ and $f^q(t)$ of pixels p and q is defined as:

$$CC = \frac{\sum_{t=0}^{N-1}[(f_t^p - \bar{f}^p)*(f_{t-r}^q - \bar{f}^q)]}{\sqrt{\sum_{t=0}^{N-1}(f_t^p - \bar{f}^p)*}\sqrt{\sum_{t=0}^{N-1}(f_{t-r}^q - \bar{f}^q)}} \quad (3)$$

where $f^p(t)$ and $f^q(t)$ are the time series values at moment t, for pixels p and q, respectively; $\bar{f}^p$ and $\bar{f}^q$ are the means of the corresponding series, r is the delay between both time

series, and N is the length of the time series. If CC is computed for $r = 0$, it estimates the time series similarity without time shift. CC values range from -1 to 1, where CC values are close to 1 in case of an increasing linear relationship. The root mean square distance (RMSD), on the other hand, is defined as:

$$RMSD = \sqrt{\frac{\sum_{t=0}^{N-1}(f_t^p - f_t^q)^2}{N^2}}. \quad (4)$$

RMSD values account for missing values by calculating only the distance between corresponding observations that are not missing. As a result, they quantify the straight-line inter-point distance in a multi-temporal space, where low values reflect high temporal similarity.

The selection of these CC and RMSD similarity measures was based on robustness to missing values. Consequently, similarity between noisy time series can be assessed by just removing outlier values. As such, the TSS_{CC} and TSS_{RMSD} approaches can be applied on the original time series without making assumptions on interpolation or curve fitting. In the proposed TSS_{CC} and TSS_{RMSD} approaches, no-data values are discarded by removing f_t^p and f_t^q values simultaneously if either one was missing. Time series with more one-third of no-data values in the one year VI^t before fire than are moreover rejected as candidate control pixels to avoid the use of time series with artificial high CC and low RMSD values due to no-data observations.

The TSS approach depends moreover strongly on the user-defined thresholds N_T and x. N_T defines the minimum number of candidate control pixels and thus shows a direct relation with the minimum window size w_{k*k} around p. Large N_T values require a large number of candidate control pixels, which results in the selection of candidate control pixels over large selection windows. x, on the other hand, defines the number of most similar control pixels. The combination of N_T and x finally determine the maximum percentage of candidate control pixels that are selected and can be determined based on the following logic. If $N_T \approx x$, control pixels will be selected over small window sizes, which is the optimal solution as the best results are obtained when control pixels are selected close to the focal pixel. However, in case that $N_T \approx x$ and there are only x candidate control pixels available, this causes a suboptimal solution. Suppose, for example, that four pixels are burnt and four pixels are un-burnt in a 3 by 3 window around a focal pixel and that $N_T = x = 4$. This situation would result in the selection of all available pixels without using the discrimination power of the VI^t time series. It is therefore advisable to select $N_T > x$ (e.g., $N_T = 2*x$). In this case, small window size is still preferentially used, but it is assured that only the 50 percent most similar candidate control pixels are used.

Analysis

The quality of control pixels as indicator for the vegetation regrowth depends entirely on how well $VI^t_{control}$ provides the temporal profile of the focal pixel VI^t_{focal} in case the fire had not occurred. Only then pRI will explain the variation caused by the regeneration process. Consequently, evaluation of the control plot selection approaches was based on un-burnt focal pixels, since the temporal similarity between VI^t_{focal} and $VI^t_{control}$ effectively can be measured after a fictive burning date. This was done by the random selection of 500 focal pixels that did not reveal any burning scar in the GBA2000 and Globscar data sets. Additionally, a fictive burning date was determined for every focal pixel by taking a random dekad in 2000, as burning dekad and considering every satellite observation before or after that date as a pre-fire and post-fire observation, respectively. Next, the un-burnt focal pixels were employed (a) to perform a sensitivity analysis of the different similarity criteria for the TSS approach, (b) to compare the proposed TSS approach with the classical control plot selection approach, and (c) to derive quality indicators for future use.

TSS Sensitivity Analysis

The selection of x and N_x, which is related to the minimum selection window size w_{k*k}, is an essential step before applying the TSS approach. This requires however an understanding of how the temporal similarity between VI^t_{focal} and $VI^t_{control}$ is affected by varying window sizes and number of selected pixels. The sensitivity of the TSS_{CC} and TSS_{RMSD} to both parameters was therefore assessed by comparing the TSS outcome for varying numbers of control pixels ($x = 1, 2, \ldots, 15$) and $N_T = \infty$. The selection of $N_T = \infty$ (for each run the set of selected candidate pixels will increase until all candidate pixels in the image are selected) in this sensitivity allows seeing how the similarity evolves over varying window sizes ($w_{k*k} | k = 3, 5, \ldots, 25$). Comparison consisted of measuring the temporal similarity for all 500 sample pixels between VI^t_{focal} and $VI^t_{control}$ over the one year pre-fire and the five year post-fire growth. For this purpose, CC and RMSD values were calculated between the focal and control pixels for the varying x and w_{k*k} values. This allows to determine how well the pre-fire temporal similarity is maintained after the fictive burning date and how the selection of x and N_T (related to w_{k*k}) influence this change.

Comparison of Control Plot Selection Approaches

The TSS approaches were subsequently contrasted with the classical REF approach. Quantitative comparison was performed to determine if the temporal similarity between VI^t_{focal} and $VI^t_{control}$ was significantly different between all approaches. Therefore, CC and RMSD values were calculated for all 500 sample pixels between the focal and control pixels of the REF_{LRLC}, TSS_{CC}, and TSS_{RMSD} approach over the five year post-fire growth for $N_x = \infty$ and varying window sizes ($w_{k*k} | k = 3, 5, \ldots, 25$).

Quality Indicators

Quality indicators are essential to assess the correctness of the pRI for future applications. The TSS approaches allow the derivation of such quality indicators based on the assumption that the time series pre-fire similarity reflects the absolute similarity between focal and control pixels. Consequently, the time series pre-fire similarity also determines the potential accuracy of the control pixels to provide the temporal profile of the focal pixel in case the fire had not occurred. This assumption was tested by comparing the pre-fire and post-fire CC and RMSD similarity values for all sample pixels.

Results

TSS Sensitivity Analysis

Figure 1 reflects the sensitivity of the TSS approaches for varying number of control pixels and selection window sizes. It shows the median temporal similarity between VI^t_{focal} and $VI^t_{control}$ of all 500 sample pixels. The median is used because it is more robust in the presence of outlier values. Figures 1a and 1b provide the one year pre-fire and five year post-fire CC values between focal and control pixels of the TSS_{CC} approach. Figures 1c and 1d contain the one

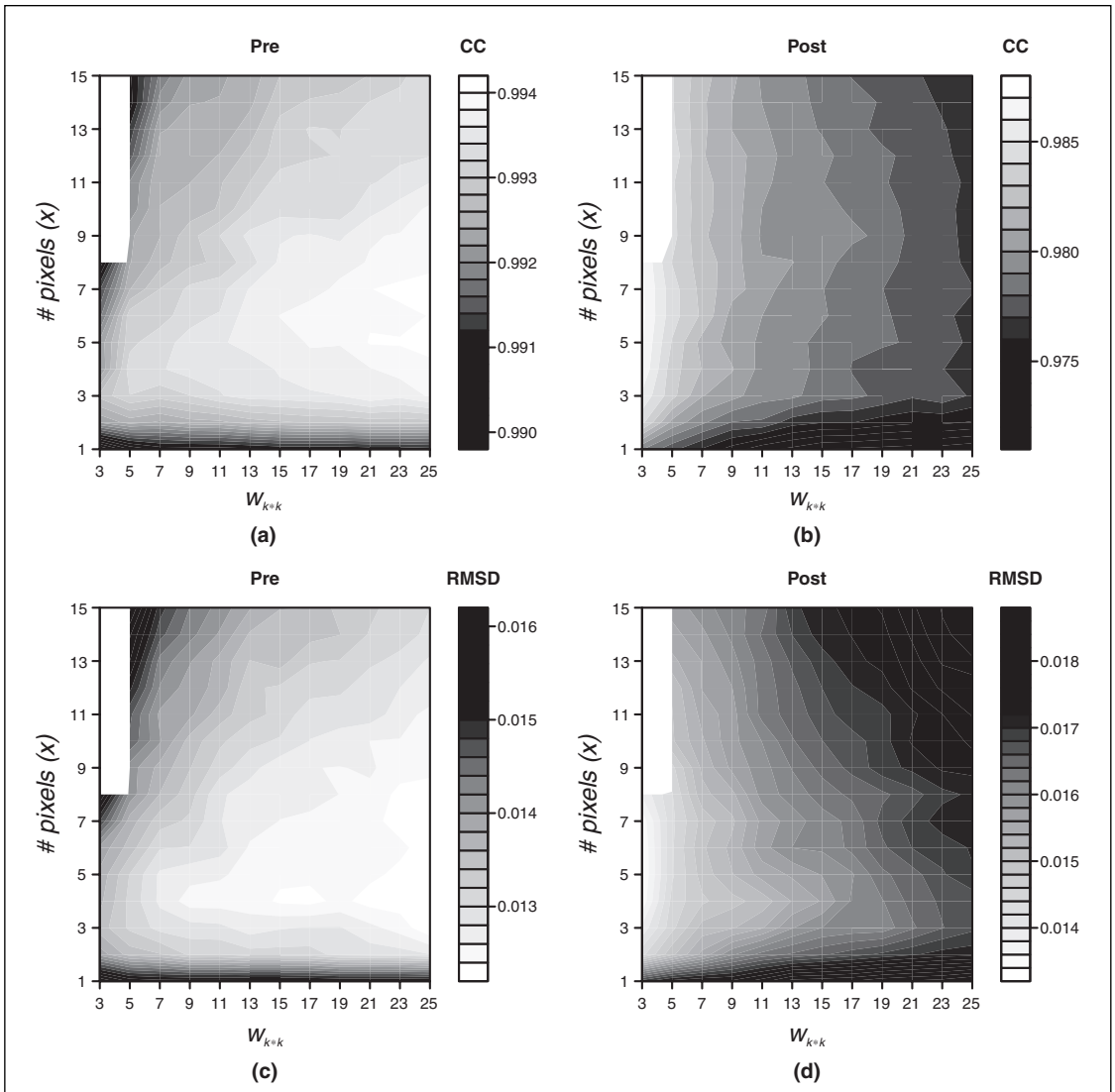

Figure 1. Sensitivity analysis of the TSS approaches in function of x and w_{k*k}. The gray scale reflects the temporal similarity, whereas white areas in upper-left corner are impossible combinations ($x > 8$ for $w_{k*k} | k = 3$): (a) pre-fire CC for TSS_{CC}, (b) post-fire CC for TSS_{CC}, (c) pre-fire RMSD for TSS_{RMSD}, and (d) post-fire RMSD for TSS_{RMSD}.

year pre-fire and five year post-fire RMSD values between focal an control pixels of the TSS_{RMSD} approach. Two main effects are observed based on the comparison of these figures. First, one can see that the difference between pre-fire similarity and post-fire similarity increases for increasing w_{k*k} values due to the window size effect. This window size effect is apparent in all four figures (Figures 1a through 1d), where the pre-fire similarity increases and post-fire similarity decreases for larger windows. This implies that, for small values, the difference between pre- and post-fire similarity is small, whereas this difference increases for increasing w_{k*k} values. Second, the number of pixels also influences the temporal similarity due to the averaging effect. This averaging effect creates an optimum in all four figures for each w_{k*k} with maximal similarities between three and six pixels.

Comparison of Control Plot Selection Approaches

Figure 2 allows to compare the control plot selection approaches, since it reflects the median temporal similarity between the VI^t_{focal} and $VI^t_{control}$ of all sample pixels for all control pixel selection approaches. Comparison of the different selection approaches shows similar patterns for all temporal similarity measures: CC (Figures 2a and 2b) and RMSD (Figures 2c and 2d). Generally, two main effects are observed. First, all lines are close together for small w_{k*k} values and diverge as w_{k*k} values increase. This means that the differences between all approaches are small for small window sizes, but increase for higher w_{k*k} values due to the window size effect. This window size effect causes a change in post-fire similarity (CC decreases and RMSD increases) for larger window sizes. The window size effect is however much stronger for the REF_{LRLC} approach than for TSS approaches. Second, comparison of the REF_{LRLC} and TSS approaches shows that high CC (Figures 2a and 2b) and low RMSD (Figures 2c and 2d) values are obtained when control pixels are selected based on the TSS_{RMSD} approach. For the other TSS approaches, on the other hand, lower similarities are obtained, whereas the REF_{LRLC} shows for all window size the lowest temporal similarity between the VI^t_{focal} and $VI^t_{control}$.

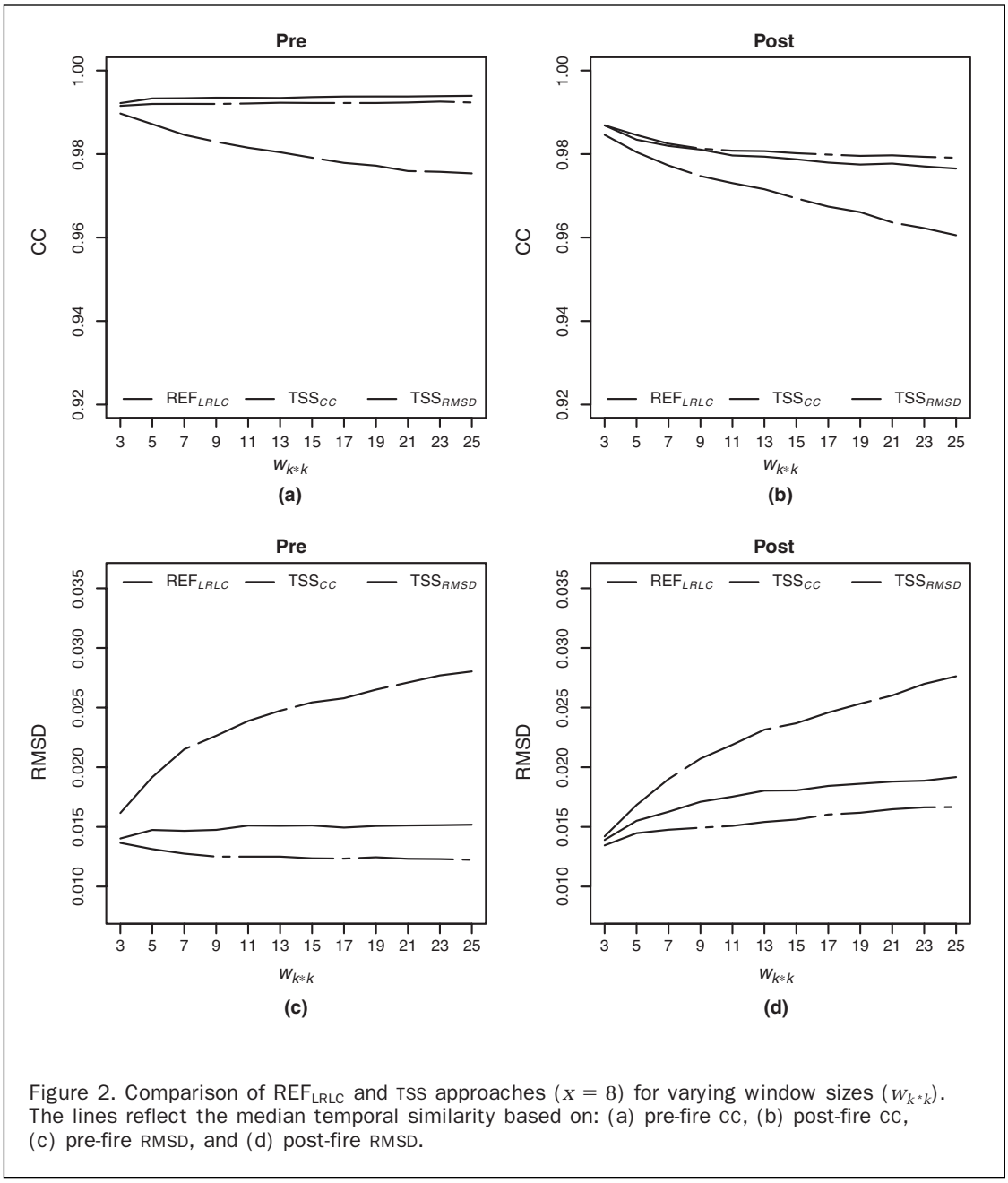

Figure 2. Comparison of REF_{LRLC} and TSS approaches ($x = 8$) for varying window sizes (w_{k^*k}). The lines reflect the median temporal similarity based on: (a) pre-fire CC, (b) post-fire CC, (c) pre-fire RMSD, and (d) post-fire RMSD.

Quality Indicators

Figure 3 shows the relation between pre- and post-fire RMSD values for all sample pixels in the TSS_{RMSD} approach with $x = 4$ and $w_{k^*k} \mid k = 7$. Hence, it reflects how the pre-fire similarity between focal and control pixel provides an indicator of the post-fire similarity. The figures for other x and w_{k^*k} values show similar patterns. Analysis of the data cloud shows a linear relationship between pre- and post-fire RMSD for the majority of the points, whereas two types of outliers give the data cloud the look of a cone. The first type of outliers is points with high pre-fire RMSD values. These are points where the TSS_{RMSD} approach fails to select control pixel that show a high similarity with the focal pixel (e.g., all points with pre-fire RMSD values above an arbitrary threshold value of 0.2). The second type of outliers is points with an elevated post-fire RMSD in comparison with their pre-fire RMSD. These are pixels where changes occurred after the fire date in the focal or control pixels as can be observed based on the comparison of points A and B in Figures 3 and 4. Figure 4 shows the time series VI^t of the focal pixel and TSS_{RMSD} control pixels plus the resulting pRI^t RMSD for points A and B in Figure 3. The time series confirm the pre- and post fire RMSD values in Figure 3 with high pre-fire similarities for A and B, high post-fire similarities for B, and low post-fire similarities for A. The time series of A show, however, a systematic difference each growing season which are not apparent in the pre-fire time series. These systematic differences cause high post-fire RMSD values, resulting in the pre-post RMSD outlier value. However, in Figure 3 one can see that this second type of outliers occurs for less than 5 percent of the pixels after thresholding. Consequently, the pre-fire RMSD can be considered with 95 percent probability as good linear indicator of the post-fire similarity, when pixels with high pre-fire RMSD values are removed (e.g., after the removal of points with pre-fire RMSD >0.2).

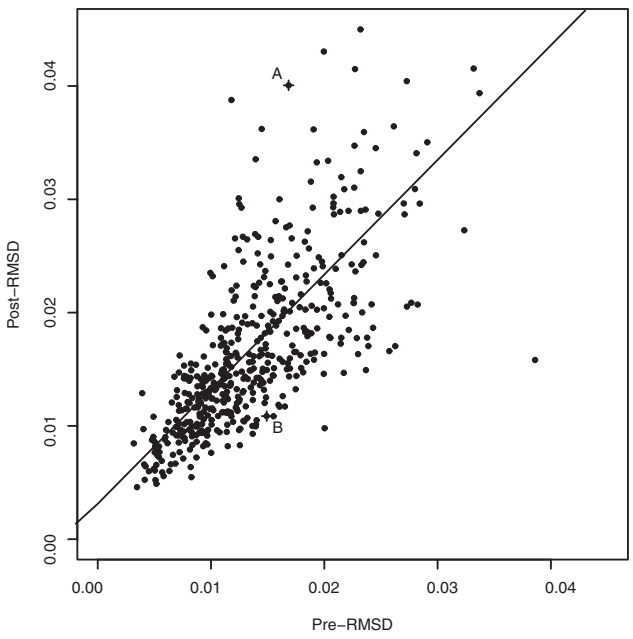

Figure 3. Time series similarity as quality indicator, which reflects the post-fire similarity (post-RMSD) in function of the post-fire similarity (post-RMSD). This figure illustrates the linear relation ship between the pre- and post-fire similarity. A and B represent two sample pixels for which the time series are shown in Figure 4.

Discussion

The objective of this research was to develop an approach for the image-based selection of control pixels for each fire pixel that allows a per-pixel regeneration index on regional, continental, or global scale. The proposed TSS approach is a spatio-temporal selection approach that employs time series similarity and spatial context to select pixels that can be used to forecast the temporal behavior of a specific focal pixel. Due to this focus on a focal pixel, only small parts of the image need to be processed as only the most similar pixels at the smallest scale are necessary for each seed pixel (burnt pixel). As a result, it is computationally efficient and can easily be applied to separate fire pixels without additional reference maps.

The quantitative comparison presented in this paper shows that the proposed TSS approaches effectively allow to select $VI^t_{control}$ that provides the temporal profile of the focal pixel VI^t_{focal} with higher accuracies than the REF approach. This better performance can be attributed to the use of the most similar pixels and not all pixels with identical reference map values in the neighborhood window. A major drawback of the reference maps at these coarse scale level is namely their broad classification rules, introducing local ecological and site differences, which impede correct application and interpretation of the RI for regrowth assessment such as in the study of Goetz *et al.* (2006). Additionally, the reference maps are often based on historical static assessments that not necessarily reflect the actual vegetation state at the moment of the fire. As a result, the REF control pixels can show a broad, within-class heterogeneity. This within-class heterogeneity is even emphasized by the window size effect that causes an increase in spatial pixel heterogeneity for expanding window sizes. The window size effect can be explained by the decrease in spatial correlation of environmental conditions when pixels are selected from larger distances. This is also apparent in the study of Lhermitte *et al.* (2008) where a decrease in temporal similarity between pixel time series is detected for increasing inter-pixel distances. The TSS approaches specifically minimize these

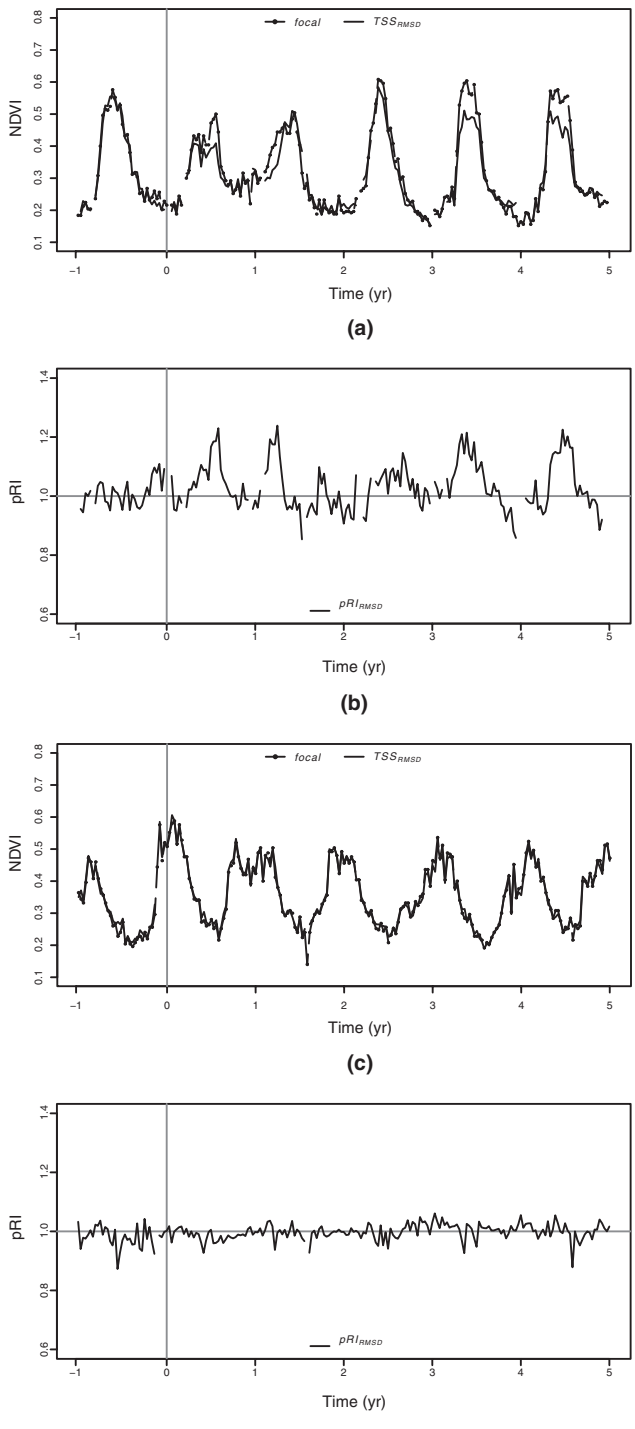

Figure 4. Illustration of time series of points A and B in Figure 3: (a) VI^t time series of A and its TSS_{RMSD} $VI^t_{control}$, (b) pRI derived from VI^t_{focal} of A and its TSS_{RMSD} $VI^t_{control}$, (c) VI^t time series of B and its TSS_{RMSD} $VI^t_{control}$, and (d) pRI derived from VI^t_{focal} of B and its TSS_{RMSD} $VI^t_{control}$.

problems of within-class heterogeneity, static reference maps and window size effects by selecting only pixels that effectively resemble the focal pixel based on similarity of the one year VI^t before fire. Nevertheless, a small window size effect is also evident for TSS approaches, namely the post-fire similarity also diminishes gently for expanding w_{k*k} values. This effect originates from the possible selection of distant pixels in large windows that have higher probabilities of showing different post-fire environmental conditions (e.g., the possibility of different weather conditions increases as the distance between pixel increases). Therefore, the best results are obtained when control pixels are selected close to the focal pixel.

Sensitivity analysis of the TSS approaches for varying number of control pixels and window sizes shows moreover that highest post-fire similarities are obtained for the VGT data set when three to six control pixels are selected ($3 \leq x \leq 6$). This is remarkable, since one would expect that the use of only the most similar pixel would give the best results. However, the noise in the original time series reduces the temporal similarity between focal and control pixels. The averaging of this noise will cause a more temporally stable signal and consequently a higher temporal similarity. On the other hand, the use of more than six pixels reduces the final similarity since non-similar pixels will also be included in the averaging process, resulting in lower post-fire similarities.

As a result of this window size and noise averaging effects, the most optimal selection of x and N_T can be derived for the TSS approaches. For the TSS_{RMSD} approach, for example, one can see in Figure 1d that when $x = 4$, the post-fire similarity shows the smallest decrease over varying window sizes. Therefore, irrespectively of N_T, the best selection of control for the TSS_{RMSD} approach over this VGT data set can be expected for $x = 4$. For other satellite sensors, vegetation types, and study areas a new sensitivity analysis may however be necessary, since the window size effect is obviously related to the spatial resolution of the satellite sensor and the spatial scale of the vegetation under study. For example, the decrease in temporal similarity between pixel time series for increasing inter-pixel distances would be less apparent when a sensor with finer spatial resolution is used over the same study area. On the other hand, very homogeneous vegetation types on a large scale will also show a smaller decrease in temporal similarity between pixel time series for increasing inter-pixel distances. As such, it is important to determine x when using different satellite sensors, vegetation types, and study areas. This can be done easily using the sensitivity analysis without the need for static reference data (as explained in the *TSS Sensitivity Analysis* sub-section). Subsequently, x can be used to determine N_T based on a user-defined maximum percentage of candidate control pixels. For example, if $N_T = 2*x$ a small window size is still preferentially used, but it is assured that only the 50 percent most similar candidate control pixels are used.

Comparison of the TSS approaches shows that the highest post-fire similarities for all similarity measures are obtained for the TSS_{RMSD} approach. This can be attributed to the different characteristics of the CC and RMSD measures. Both measures are dependent upon shape transformations including amplitude scaling, time translations, and noise, but the CC is invariant for amplitude translations (Liao, 2005). As a result, CC fails to detect amplitude translations or absolute offsets between time series, thus allowing time series with similar shapes and different vertical offsets to be classified similar. Amplitude translation would result from differing backgrounds, e.g., different soil types or understory vegetation (Evans and Geerken, 2006), which are important for regrowth monitoring.

Due to all these effects, TSS_{RMSD} with $x = 4$ and $N_T = 8$ provides the most optimal approach to select control pixels for the VGT data set in the study area. Further research is now necessary in order to effectively apply the pRI methods on burnt pixels, since this will allow quantifying the vegetation regrowth for each pixel on a large scale. For example, in Figure 5 the pRI is illustrated showing the fire impact on three different Globscar fire pixels in the study area, reflecting increasing levels of fire impact. Quantifying and understanding these three levels of severity should however be the next step of current research.

Analysis of the pre- and post-fire temporal similarities for the optimal TSS_{RMSD} approach indicates furthermore that the pre-fire RMSD similarity values reflect the absolute similarity between focal and control pixels, except for outlier values. Consequently, the pre-fire similarity values can be considered as a quality indicator for the pRI. As such, they can be used to prevent the use of the pRI for focal pixels where no good control pixels can be derived, namely when low pre-fire RMSD values are obtained. By applying a threshold value on these pre-fire RMSD values, these types of outliers can be removed.

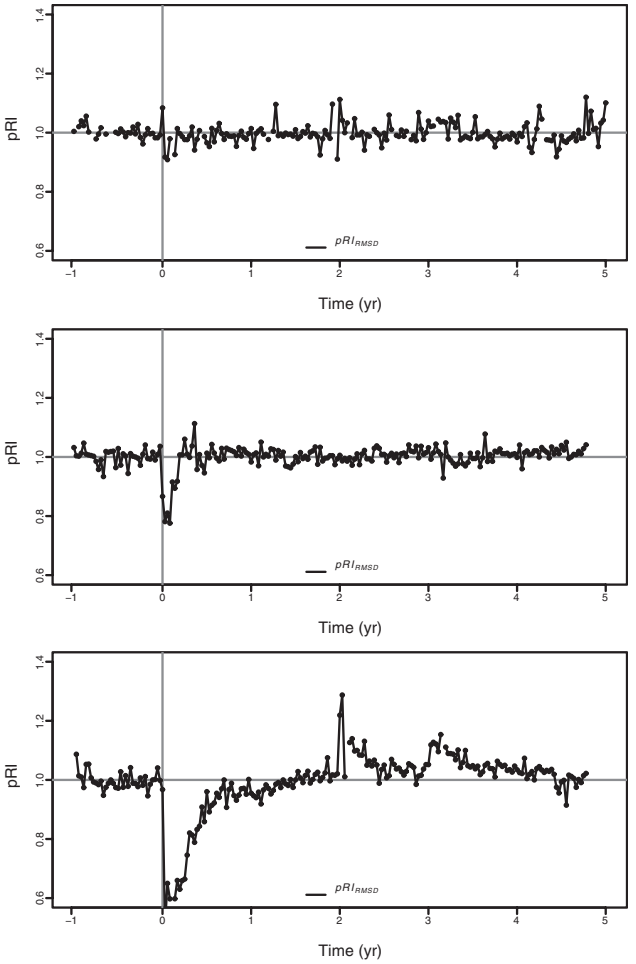

Figure 5. Illustration of the pRI based on TSS_{RMSD} with $x = 4$ and $N_T = 8$ control pixels for three sample pixels. Each figure shows the fire impact of a different pixel in the study area, and reflects an increasing level of fire impact.

This requires however calibration for each data set over different geographic areas. This calibration can be performed by analyzing the pre- and post-fire RMSD for unburnt pixels in a linear regression and defining a pre-fire RMSD threshold value below which few outlier values occur. For the presented data set, for example, one can see that, for an arbitrary pre-fire RMSD = 0.2 threshold value, the validity of the remaining pRI values can be considered with 95 percent accuracy, since only 5 percent are apparent outlier values. This implies that for the pixels with an acceptable pre-fire RMSD value below the threshold, a 5 percent probability exists for post-fire changes that corrupt the pRI^t interpretation. These post-fire changes are caused by the selection of control pixels based on the pre-fire temporal characteristics, whereas all kinds of changes can occur afterwards that diminish the temporal similarity in the post-fire time series. However, the incorporation of additional change maps over time such as developed by Linderman *et al.* (2005) can reduce the chance of selecting such changed pixels even more for future applications. Consequently, the basic assumption of the pRI, namely that control plots can serve as an indicator for vegetation growth in case the fire had not occurred, can be maximized and the pRI can be applied to a range of remote sensing derived time series of different kinds of sensors (e.g., other indices or individual spectral bands) to monitor in real-time the vegetation regrowth after large scale fires.

Moreover, the image based selection approach for control pixels based on time series similarity (TSS) is not restricted to burnt areas. The pRI and TSS approaches are generalized approaches that can be applied to any type of disturbance or change based on any multi-temporal data set. As such, they can contribute to obtain a better understanding of factors affecting land-use and land-cover resulting in potential climate warming, land degradation and bio-diversity loss. The only basic requirement to use the pRI approach for such disturbance, would be that (a) the user has a clear understanding of the meaning of pRI, namely that control plots can serve as an indicator for the change caused by the disturbance, and (b) the normal situation, namely the vegetation growth of the control pixels without disturbance, is a meaningful indicator to compare with the disturbance with. The latter, for example, is not the case when vegetation growth goes through completely different states.

Conclusions

The objective of this study was the development of an automatic selection approach of control pixels for pixels that allows for calculation of a pixel-based regeneration index. The introduction of the time series similarity (TSS) approaches showed that the selection of the control pixels based on similarity of the one year VI^t before fire, provides a valuable alternative for the REF approach based on reference maps. The TSS approaches specifically minimize the drawbacks of the REF approach, namely the within-class heterogeneity and dependence of static reference data, by selecting only pixels that effectively resemble the focal pixel based on similarity of the one year VI^t before fire. Comparison of the TSS approaches showed moreover that the highest post-fire similarities were obtained for the TSS_{RMSD} approach with $x = 4$ and $N_T = 8$ due to beneficial averaging effects and minimal window size effects. As such, the effects of spatial heterogeneity and noise are minimized and the control pixels provide optimally the temporal profile of the focal pixel VI^t focal in case the fire had not occurred. Pre-fire RMSD values of the control pixels of the TSS_{RMSD} approach allowed moreover deriving the quality of the control pixels before using them in pRI calculations. As a result, the wrong use of the pRI can be avoided by applying a threshold value on these pre-fire RMSD values, since the low pre-fire similarities reflect the inability to serve as a good indicator of post-fire growth. Further research is necessary in order to effectively apply the pRI on burnt pixels and to monitor the vegetation regrowth for each pixel on a large scale. Consequently, indicators for spatio-temporal post-fire development can be derived to understand the impact of vegetation fires and to estimate the changes of terrestrial ecosystems after fire. In future research, focus will be on the derivation of one of such indicators.

Acknowledgments

This work was performed in the framework of a research project on satellite remote sensing of terrestrial ecosystem dynamics, funded by the Belgian Science Policy Office. The SPOT VGT S10 data set was generated by the Vlaamse Instelling voor Technologisch Onderzoek (VITO), whereas the National Land Cover Map of South Africa was supplied by the Agricultural Research Council (ARC). We are indebted to the editor and referees for their detailed reviews that led to an improved version of the manuscript.

References

Alleaume, S., C. Hély, J. Le Roux, S. Korontzi, R.J. Swap, H.H. Shugart, and C.O. Justice, 2005. Using MODIS to evaluate heterogeneity of biomass burning in southern African savannahs: A case study in Etosha, *International Journal of Remote Sensing*, 36(19): 4219–4237.

Chuvieco, E., 1999. Measuring changes in landscape pattern from satellite images: Short-term effects of fire on spatial diversity, *International Journal of Remote Sensing*, 20(12): 2331–2346.

Cihlar, J., 2000. Land cover mapping of large areas from satellites: Status and research Properties, *International Journal of Remote Sensing*, 21(6–7):1093–1114.

Defries, R.S., M.C. Hansen, and J.R.G. Townshend, 1995. Global discrimination of land cover types from metrics derived from AVHRR pathfinder data, *Remote Sensing of Environment*, 54:209–222.

Díaz-Delgado, R., F. Lloret, and X. Pons, 2003. Influence of fire severity on plant regeneration by means of remote sensing imagery, *International Journal of Remote Sensing*, 24(8): 1751–1763.

Díaz-Delgado, R., and X. Pons, 2001. Spatial patterns of forest fires in Catalonia NE of Spain along the period 1975–1995 - Analysis of vegetation recovery after fire, *Forest Ecology and Management*, 147(1):67–74.

Díaz-Delgado, R., R. Salvador, and X. Pons, 1998. Monitoring of plant community regeneration after fire by remote sensing, *Fire Management and Landscape Ecology* (L. Traboud, editor), International Association of Wildland Fire, Fairfield, Washington, pp. 315–324.

Ehrlich, D., E.F. Lambin, and J.P. Malingreau, 1997. Biomass burning and broad-scale land-cover changes in Western Africa, *Remote Sensing of Environment*, 61(2):201–209.

Espírito-Santo, F.D.B., Y.E. Shimabukuro, and T.M. Kuplich, 2005. Mapping forest successional stages following deforestation in Brazilian Amazonia using multi-temporal Landsat images, *International Journal of Remote Sensing*, 26(3):635–642.

Evans, J.P., and R. Geerken, 2006. Classifying rangeland vegetation type and coverage using a Fourier component based similarity measure, *Remote Sensing of Environment*, 105:1–8.

Fiorella, M., and W.J. Ripple, 1993. Analysis of conifer forest regeneration using Landsat Thematic Mapper, *Photogrammetric Engineering & Remote Sensing*, 59(9):1383–1388.

Fraser, R.H., Z. Li, and R. Landry, 2000. SPOT VEGETATION for characterizing boreal forest Fires, *International Journal of Remote Sensing*, 21(18):3525–3532.

Goetz, S.J., G.J. Fiske, and A.G. Bunn, 2006. Using satellite time-series data sets to analyze fire disturbance and forest recovery across Canada, *Remote Sensing of Environment*, 101(3):352–365.

Hayes, D.J., and S.A. Sader, 2001. Comparison of change-detection techniques for monitoring tropical forest clearing and vegetation regrowth in a time series, *Photogrammetric Engineering & Remote Sensing*, 67(9):1067–1074.

Henry, M.C., and A.S. Hope, 1998. Monitoring post-burn recovery of chaparral vegetation in southern California using multi-temporal satellite data, *International Journal of Remote Sensing*, 19(16):3097–3107.

Hicke, J.A., G.P. Asner, E.S. Kasischke, N.H.F. French, J.T. Randerson, G.J. Collatz, B.J. Stocks, C.J. Tucker, S.O. Los, and C.B. Field, 2003. Postfire response of North American boreal forest net primary productivity analyzed with satellite observations, *Global Change Biology*, 9(8):1145–1157.

Holben, B.N., 1986. Characterization of maximum value composites from temporal AVHRR Data, *International Journal of Remote Sensing*, 7:1417–1434.

Justice, C.O., J.R.G. Townshend, B.N. Holben, and C.J. Tucker, 1985. Analysis of the phenology of global vegetation using meteorological satellite data, *International Journal of Remote Sensing*, 6(8):1271–1318.

Kempeneers, P., G. Lissens, F. Fierens, and J. Van Rensbergen, 2000. Development of a cloud, snow and cloud shadow mask for VEGETATION imagery, *Proceedings of the IGARSS Geoscience and Remote Sensing Symposium 2000*, July, Honolulu, Hawaii, pp. 834–836.

Kushla, J.D., 1998. Assessing wildfire effects with Landsat thematic mapper data, *International Journal of Remote Sensing*, 19(13):2493–2507.

Lambin, E. F., K. Goyvaerts, and C. Petit, 2003. Remotely-sensed indicators of burning efficiency of savannah and forest fires, *International Journal of Remote Sensing*, 24(15):3105–3118.

Lawrence, R.L., and W.J. Ripple, 1999. Calculating change curves for multitemporal satellite imagery: Mount St. Helens 1980–1995, *Remote Sensing of Environment*, 67(3):309–319.

Lhermitte, S., J. Verbesselt, J. Jonckheere, J.A.N. van Aardt, K. Nackaerts, W.W. Verstraeten, and P. Coppin, 2008. Hierarchical image segmentation based on similarity of NDVI time series. *Remote Sensing of Environment*, 112(2):506–521.

Liao, T., 2005. Clustering of time series data - A survey, *Pattern Recognition*, 38:1857–1874.

Linderman, M., P. Rowhani, D. Benz, S. Serneels, and E. Lambin, 2005. Land-cover change and vegetation dynamics across Africa, *Journal of Geophysical Research*, 110(D12104):doi:10.1029/2004JD005521.

Loveland, T.R., B.C. Reed, J.F. Brown, D.O. Ohlen, Z. Zhu, L. Yang, and J.W. Merchant, 2000. Development of a global land cover characteristics database and IGBP DISCover from 1 km AVHRR data, *International Journal of Remote Sensing*, 21(6–7): 1303–1330.

Low, A.B., and A.G. Rebelo, 1996. *Vegetation of South Africa, Lesotho, and Swaziland*, Department of Environmental Affairs and Tourism, Pretoria, South Africa, pp. 93–103.

Marchetti, M., C. Ricotta, and F. Volpe, 1995. A qualitative approach to the mapping of postfire regrowth in Mediterranean vegetation with Landsat TM data, *International Journal of Remote Sensing*, 16(13):2487–2494.

Rahman, H., and G. Dedieu, 1994. SMAC: A simplified method for the atmospheric correction of satellite measurements in the solar spectrum, *International Journal of Remote Sensing*, 15:123–143.

Reed, B.C., J.F. Brown, D. Vanderzee, T.S. Loveland, J.W. Merchant, and D.O. Ohlen, 1994. Measuring phenological variability from satellite imagery, *Journal of Vegetation Science*, 5:703–714.

Riaño, D., E. Chuvieco, S. Ustin, R. Zomer, P. Dennison, D. Roberts, and J. Salas, 2002. Assessment of vegetation regeneration after fire through multitemporal analysis of AVIRIS images in the Santa Monica Mountains, *Remote Sensing of Environment*, 79(1):60–71.

Ricotta, C., 1998. Monitoring the landscape stability of Mediterranean vegetation in relation to fire with a fractal algorithm, *International Journal of Remote Sensing*, 19(5):871–881.

Silva, J.M.N., J.M. Pereira, A. Cabral, A.C.L. Sá, M.J.P. Vasconcelos, B. Mota, and J.-M. Grégoire, 2003. An estimate of the area burned in southern Africa during the 2000 dry season using SPOT- VEGETATION satellite data, *Journal of Geophysical Research*, 108(D13): doi.10.1029/2002JD002320.

Simon, M., S. Plummer, F. Fierens, J.J. Hoelzemann, and O. Arino, 2004. Burnt area detection at global scale using ATSR-2: The GLOBSCAR products and their qualification, *Journal of Geophysical Research*, 109(D14S02): doi:10.1029/2003JD003622.

Song, C.H., 2002. The spectral/temporal manifestation of forest succession in optical imagery - The potential of multitemporal imagery, *Remote Sensing of Environment*, 82(2–3):285–302.

Song, C.H., 2003. Monitoring forest succession with multitemporal Landsat images: Factors of Uncertainty, *IEEE Transactions on Geoscience and Remote Sensing*, 41(11):2557–2567.

Tainton, N., 1999. *Veld Management in South Africa*, University of Natal Press, Pietermaritzburg, South Africa.

Thompson, M.W., 1999. *South African National Landcover Database Project, Data Users Manual: Final Report (Phases 1, 2, and 3)*, Client Report ENV/P/C 98136, CSIR, Pretoria, South Africa.

van Wilgen, B.W., and R.J. Scholes, 2000. The vegetation and fire regimes of southern hemisphere Africa, *Fire in Southern African Savannas: Ecological and Atmospheric Perspectives* (B.W. van Wilgen, M.O. Andreae, J.G. Goldammer, and J.A. Lindesay, editors), Witwatersrand University Press, Johannesburg, South Africa, pp. 27–36.

Verbesselt, J., B. Somers, J. van Aardt, I. Jonckheere, and P. Coppin, 2006. Monitoring herbaceous biomass and water content with SPOT VEGETATION time-series to improve fire risk assessment in savanna ecosystems, *Remote Sensing of Environment*, 101(3):399–414.

Viedma, O., J. Meliá, D. Segarra, and J. García-Haro, 1997. Modeling rates of ecosystem recovery after fires by using Landsat TM data, *Remote Sensing of Environment*, 61(3):383–398.

Viovy, N., 2000. Automatic Classification of Time Series (ACTS): A new clustering method for remote sensing time series, *International Journal of Remote Sensing*, 21(6–7):1537–1560.

White, J.D., K.C. Ryan, C.C. Key, and S.W. Running, 1996. Remote sensing of forest fire severity and vegetation recovery, *International Journal of Wildland Fire,* 6(3):125–136.

(Received 06 March 2008; accepted 14 January 2009; final version 25 September 2009)